

# Electronic Supplementary Information: Interactions between brush-grafted nanoparticles within chemically identical homopolymers: the effect of brush polydispersity

So Jung Park, Daeseong Yong, and Jaeup U. Kim\*

*Department of Physics, School of Natural Science,  
Ulsan National Institute of Science and Technology (UNIST), Ulsan 44919, Republic of Korea*

Seyong Kim and Joona Bang†

*Department of Chemical and Biological Engineering,  
Korea University, Seoul 02841, Republic of Korea*

Youngson Choe

*Department of Chemical Engineering, Pusan National University, Busan, 46241, Republic of Korea*

## A. Additional Experimental Information

### Material

Styrene and methyl methacrylate (MMA) monomers were purchased from Aldrich and purified by passing through a basic alumina column. 2,2'-azobis(isobutyronitrile) (AIBN), 4-vinylbenzyl chloride, tetraoctylammonium bromide (TOAB), hexyl amine, anhydrous tetrahydrofuran (THF), dimethylformamide (DMF), hexane, 1,4-dioxane, dichloromethane (DCM) and methanol were purchased from Sigma Aldrich and used as received without further purification. Polystyrene (PS) and poly(methyl methacrylate) (PMMA) homopolymers were purchased from Polymer Source Inc. and used as received without further purification.

### Synthesis of polymeric ligands

Various thiol-terminated photo cross-linkable polymeric ligands were synthesized by reversible addition fragmentation transfer (RAFT) polymerization as described elsewhere

---

\*Electronic address: [jukim@unist.ac.kr](mailto:jukim@unist.ac.kr)

†Electronic address: [joona@korea.ac.kr](mailto:joona@korea.ac.kr)

[1, 2]. For P(MMA-*b*-S-N<sub>3</sub>)-SH, PMMA selective ligands, mixtures of MMA, RAFT agent and AIBN were purged with nitrogen gas in a Schlenk flask, and then polymerized at 70 °C for 4 hours to obtain PMMA-RAFT macroinitiators. For the second block, PMMA-RAFT, 4-vinylbenzyl chloride and AIBN were mixed and purged with nitrogen gas, and then polymerized at 70 °C for 10 hours to produce P(MMA-*b*-S-Cl)-RAFT. For substitution reaction, P(MMA-*b*-S-Cl)-RAFT was dissolved in dry THF with hexyl amine, and then purged with nitrogen gas. The reaction was performed at room temperature until solution color changes from red to pale yellow. The mixture was precipitated into methanol to obtain P(MMA-*b*-S-Cl)-SH. The thiol terminated polymer was dissolved in DMF with sodium azide, and then the solution was stirred for 24 hours. The resulting polymer, P(MMA-*b*-S-N<sub>3</sub>)-SH was precipitated in methanol and dried in vacuum. P[S-*b*-(S-*r*-S-N<sub>3</sub>)]-SH was synthesized using the same procedure explained above, but the second block was randomly copolymerized with styrene and 4-vinylbenzyl chloride with the feed mole ratio of 7:3. The number-averaged molecular weights ( $M_n$ 's) and polydispersity index (PDI) of synthesized polymeric ligands are listed in Table 1 in the main text.

### **Synthesis of Au NPs with synthesized photo cross-linkable ligands**

The Au NPs were synthesized with various polymeric ligands via two phase method as described elsewhere [1, 2]. During the synthesis of Au NPs, the mole feed ratio between the polymeric ligands and Au atoms was kept at 0.3. To remove unattached free chains, TOAB, and residual reducing agents, Au NPs were precipitated in mixture of hexane and methanol at least five times. The Au NPs were re-dispersed in UV transparent solvent, 1,4-dioxane. The solutions were then exposed to UV light ( $\lambda = 254$  nm) for 1 hour under ambient condition for crosslinking the shell. The transmission electron microscopy (TEM) images of the synthesized Au NPs are shown in Figure S1.

### **Preparation of homopolymer/Au NP bulk nanocomposites**

For the homopolymer template, PS and PMMA were used. A series of DCM/PS solutions, each containing 2 wt% PS of different molecular weight ( $M_n = 24,000$  g/mol, 61,000 g/mol and 93,000 g/mol) were mixed with PS selective Au NPs which have different length of ligands, of concentrations 10 wt% to PS homopolymer matrix. The solutions are then drop-cast onto sodium chloride (NaCl) substrates to make bulk state nanocomposites.

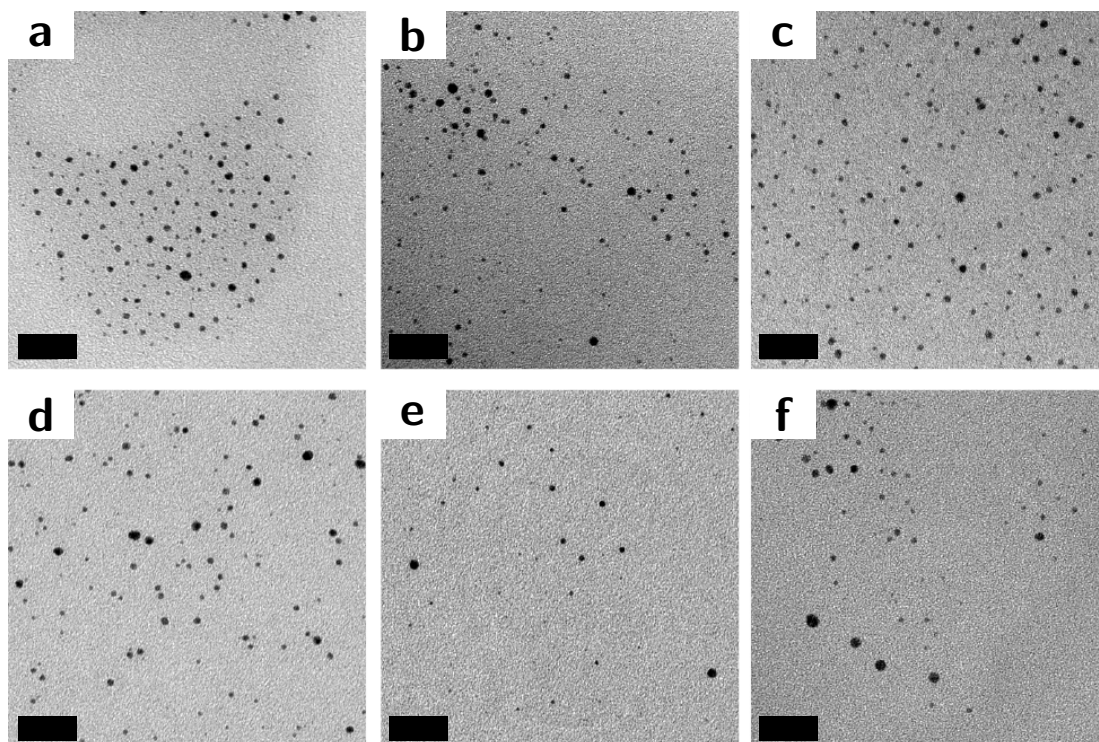


Figure S1: TEM images of synthesized (a) Au-PS-6K, (b) Au-PS-9K, (c) Au-PS-22K, (d) Au-PMMA-5.3K, (e) Au-PMMA-11K, and (f) Au-PMMA-27K, respectively. Scale bar is 30 nm.

Samples were in an ambient condition for a day for solvent evaporation and then annealed in a vacuum oven at 200 °C for 48 hours. Due to the thermal stability of shell crosslinked Au NPs, the annealing under this condition would lead the system to reach an equilibrium state without agglomeration of NPs. In the case of PMMA based nanocomposites, we used PMMA with three different molecular weights ( $M_n = 24,000$  g/mol, 60,000 g/mol and 95,000 g/mol) as matrices, and the nanocomposites were prepared with the same procedure described above.

### Characterization

The size of Au NPs and their dispersion in the homopolymer matrix were examined by TEM. To determine the dispersion of Au NPs in the polymer matrix, the annealed samples were microtomed into 70 – 80 nm slices for cross-sectional TEM analysis.

## B. Mean Field Density and Free Energy of the Two Particle System

In this section, we discuss the detailed derivation of the mean field segment density and the free energy expression for the homopolymers and brush chains grafted to two particles. We begin with the expression of the formal partition function of the system, shown as eq (2) in the main text. A functional integral  $\int \mathcal{D}\Phi_f \delta[\Phi_f - \hat{\phi}_f]$  is inserted to replace the chain conformation dependent density function  $\hat{\phi}_f$  with the ordinary function  $\Phi_f$  [3],

$$Z \propto \frac{1}{n_g!n_f!} \int \mathcal{D}\Phi_f \prod_{i=1}^{n_g} \mathcal{D}\mathbf{r}_{g,i} P[\mathbf{r}_{g,i}] \prod_{j=1}^{n_f} \mathcal{D}\mathbf{r}_{f,j} P[\mathbf{r}_{f,j}] \\ \times (\delta(r_{g,i}(1) - R) + \delta(\bar{r}_{g,i}(1) - R)) \delta[1 - \hat{\phi}_g - \Phi_f] \delta[\Phi_f - \hat{\phi}_f] \quad (\text{B1})$$

The two delta functionals are now replaced with integral representations by using

$$\delta[f] \propto \int \mathcal{D}W \exp\left(\frac{\rho_0}{N} \int d\mathbf{r} W(\mathbf{r}) f(\mathbf{r})\right) \quad (\text{B2})$$

where  $W_g$  and  $W_f$  are used for the first and second delta functions, respectively, and the  $W$  integrations are along the imaginary axis. The density functions  $\hat{\phi}_g$  and  $\hat{\phi}_f$  are substituted with their definitions in eqs (3) and (4) in the main text, respectively, and the result of the algebraic transform is

$$Z \propto \frac{1}{n_g!n_f!} \int \mathcal{D}\Phi_f \prod_{i=1}^{n_g} \mathcal{D}\mathbf{r}_{g,i} P[\mathbf{r}_{g,i}] \prod_{j=1}^{n_f} \mathcal{D}\mathbf{r}_{f,j} P[\mathbf{r}_{f,j}] (\delta(r_{g,i}(1) - R) + \delta(\bar{r}_{g,i}(1) - R)) \\ \times \int \mathcal{D}W_g \exp\left[\frac{\rho_0}{N} \int d\mathbf{r} W_g(1 - \Phi_f)\right] \exp\left[-\sum_{i=1}^{n_g} \int_0^1 ds W_g(\mathbf{r}_{g,i}(s))\right] \\ \times \int \mathcal{D}W_f \exp\left[\frac{\rho_0}{N} \int d\mathbf{r} W_f \Phi_f\right] \exp\left[-\sum_{j=1}^{n_f} \int_0^\alpha ds W_f(\mathbf{r}_{f,j}(s))\right] \quad (\text{B3})$$

The above equation can be rewritten as

$$Z \propto \frac{1}{n_g!n_f!} \int \mathcal{D}W_g \mathcal{D}W_f \mathcal{D}\Phi_f \left(\frac{\rho_0}{N} Q_g[W_g]\right)^{n_g} \left(\frac{\rho_0}{\alpha N} Q_f[W_f]\right)^{n_f} \\ \times \exp\left(\frac{\rho_0}{N} \int d\mathbf{r} W_g(1 - \Phi_f) + \frac{\rho_0}{N} \int d\mathbf{r} W_f \Phi_f\right) \quad (\text{B4})$$

where  $Q_\kappa[W_\kappa]$  are the single chain partition functions for both grafted chain ( $\kappa = g$ ) and

free chain ( $\kappa = f$ ) subjected to the external fields,  $W_\kappa(\mathbf{r})$ , as follows:

$$Q_g[W_g] \propto \int \mathcal{D}\mathbf{r} (\delta(r(1) - R) + \delta(\bar{r}(1) - R)) \times \exp \left[ -\frac{3}{2a^2N} \int_0^1 ds |\mathbf{r}'(s)|^2 - \int_0^1 ds W_g(\mathbf{r}(s)) \right] \quad (\text{B5})$$

$$Q_f[W_f] \propto \int \mathcal{D}\mathbf{r} \exp \left[ -\frac{3}{2a^2N} \int_0^\alpha ds |\mathbf{r}'(s)|^2 - \int_0^\alpha ds W_f(\mathbf{r}(s)) \right] \quad (\text{B6})$$

It is customary to extract factors  $(\rho_0/N)^{n_g}$  and  $(\rho_0/\alpha N)^{n_f}$  from the unspecified proportionality constant in eq (B4) for future simplification [3]. After applying Stirling approximation ( $\ln(n_\kappa!) \approx n_\kappa \ln n_\kappa - n_\kappa$ ) on the factorials, the partition function of the system can be reexpressed as

$$Z \propto \int \mathcal{D}W_g \mathcal{D}W_f \mathcal{D}\Phi_f \exp \left( -\frac{F[W_g, W_f, \Phi_f]}{k_B T} \right) \quad (\text{B7})$$

$$\frac{F}{k_B T} = n_g \left( \ln \left( \frac{V_g}{Q_g[W_g]} \right) - 1 \right) + n_f \left( \ln \left( \frac{V_f}{Q_f[W_f]} \right) - 1 \right) - \frac{\rho_0}{N} \int d\mathbf{r} [W_g(1 - \Phi_f)] - \frac{\rho_0}{N} \int d\mathbf{r} [W_f \Phi_f] \quad (\text{B8})$$

where  $V_g \equiv n_g N / \rho_0$  and  $V_f \equiv \alpha n_f N / \rho_0$ .

In the standard self-consistent field theory (SCFT) formulation, mean field solutions are obtained by applying the saddle point approximation which is asymptotically exact in the limit of very long chains. In this approach, the exponent in eq (B7) is minimized by functional derivative with respect to the three field variables,  $W_g$ ,  $W_f$  and  $\Phi_f$  as follows:

$$\frac{\mathcal{D}F(W_g, W_f, \Phi_f)}{\mathcal{D}W_f} = 0 \quad (\text{B9})$$

$$\frac{\mathcal{D}F(W_g, W_f, \Phi_f)}{\mathcal{D}W_g} = 0 \quad (\text{B10})$$

$$\frac{\mathcal{D}F(W_g, W_f, \Phi_f)}{\mathcal{D}\Phi_f} = 0 \quad (\text{B11})$$

From now on, we will use lowercase functions  $w_g$ ,  $w_f$  and  $\phi_f$  for the saddle point solution of the above equations. The first functional derivative, eq (B9), reduces to

$$\phi_f(\mathbf{r}) = -\frac{V_f}{\alpha} \frac{\mathcal{D} \ln(Q_f[w_f])}{\mathcal{D}w_f(\mathbf{r})} = \left\langle \hat{\phi}_f(\mathbf{r}) \right\rangle \quad (\text{B12})$$

which identifies the mean field function  $\phi_f(\mathbf{r})$  as the ensemble average segment density of  $\hat{\phi}_f(\mathbf{r})$  at the mean field  $w_f(\mathbf{r})$ . The second functional derivative, eq (B10), leads to

$$1 - \phi_f(\mathbf{r}) = -V_g \frac{\mathcal{D} \ln(Q_g[w_g])}{\mathcal{D}w_g(\mathbf{r})} = \left\langle \hat{\phi}_g(\mathbf{r}) \right\rangle \quad (\text{B13})$$

which implies the incompressibility condition

$$\phi_g(\mathbf{r}) + \phi_f(\mathbf{r}) = 1 \quad (\text{B14})$$

where  $\phi_g$  is the ensemble average segment density of  $\hat{\phi}_g(\mathbf{r})$  at the mean field  $w_g(\mathbf{r})$ . The third functional derivative, eq (B11), produces

$$w_g(\mathbf{r}) = w_f(\mathbf{r}) \quad (\text{B15})$$

This relation is not as trivial as one might think at first glance. It is true only when the continuous parameter  $s$  of the free chain goes from 0 to  $\alpha$ . There is another approach of using the parameter range  $[0,1]$ , which results in  $w_f(\mathbf{r})$  larger than  $w_g(\mathbf{r})$  by a factor  $\alpha$ .

After all the segment densities and mean potential fields are obtained, the mean field free energy for the system is,

$$\frac{F}{k_B T} = n_g \left( \ln \left( \frac{V_g}{Q_g[w]} \right) - 1 \right) + n_f \left( \ln \left( \frac{V_f}{Q_f[w]} \right) - 1 \right) - \frac{\rho_0}{N} \int d\mathbf{r} w(\mathbf{r}) (\phi_g(\mathbf{r}) + \phi_f(\mathbf{r})) \quad (\text{B16})$$

where the subscripts for the fields are omitted. With the current expression, when we take larger system size by adding more free homopolymer chains, the free energy varies due to the increase of the free chain numbers as implied by the term  $-1$  in the second parenthesis. When we consider effective interaction between two particles, the system size varies with the interparticle distance  $D$ , and the system size dependent free energy expression is inappropriate. For this reason, we adopt the following free energy expression which is independent of the system size,

$$\frac{F}{k_B T} = n_g \ln \left( \frac{V_g}{Q_g[w]} \right) + n_f \ln \left( \frac{V_f}{Q_f[w]} \right) - \frac{\rho_0}{N} \int d\mathbf{r} w(\mathbf{r}) (\phi_g(\mathbf{r}) + \phi_f(\mathbf{r})) \quad (\text{B17})$$

With this form, the free energy value converges to a finite value as the system size diverges by adding infinitely many free chains, thus this excess free energy expression provides the proper interparticle interaction potential in the homopolymer background.

### C. Brush Morphology of Isolated Particle

For the preparation of the study of the two-particle interaction, we present the analysis of an isolated particle system (i.e.,  $D \rightarrow \infty$ ) in this section. When there is no chemical distinction between the polymer chains, the interaction between two particles purely originates from entropic contributions of the polymer chains. There are two main entropic contributions; one is the conformational entropy of brush polymers and the other is the translational entropy of free polymers. Competition between these two types of entropic effects determines the morphology of the system. We begin the analysis by examining the segment density profile, and our focus is on how parameters such as particle radius  $R$ , brush thickness  $H_{\text{brush}}$  and chain length ratio  $\alpha$  affect the properties of the interface between the brush and the free chains.

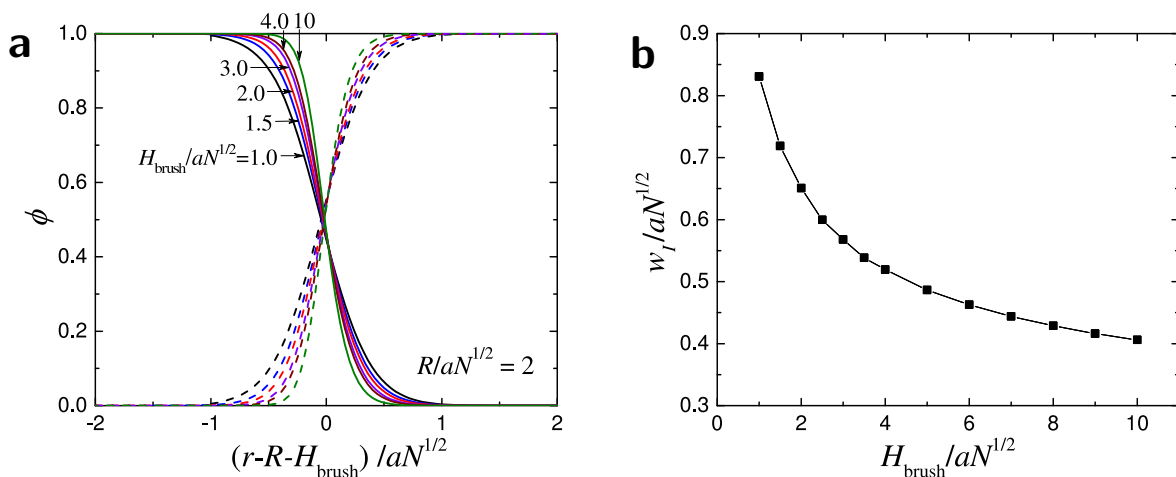


Figure S2: (a) Segment density profiles of grafted polymers ( $\phi_g$ , solid lines), and free polymers ( $\phi_f$ , dashed lines), and (b) corresponding interfacial width  $w_I$ , for a particle with radius  $R = 2aN^{1/2}$  at various brush thicknesses  $H_{\text{brush}}$ . The length of the two types of polymers are the same ( $\alpha = 1$ ).

In Figure S2a, we display density profiles of the grafted and free polymers on an isolated particle of radius  $R = 2aN^{1/2}$  at various  $H_{\text{brush}}$  values. The brush height,  $H_{\text{brush}}$ , is defined as the thickness of the brush layer in the absence of the free polymer penetration. Sparsely grafted brush is represented by a small  $H_{\text{brush}}$ , and its value increases as the grafting density increases. In the experiment section of the main text, our discussion was focused on the grafting density, but  $H_{\text{brush}}$  is a parameter easier to control in the theoretical analysis; thus,

we use  $H_{\text{brush}}$  as the main parameter in this paper.

In order to focus on the geometrical effect, we fix  $\alpha = 1$  for this and the next figure. As shown in Figure S2a, at increasing  $r$ , the brush-rich phase changes to the free polymer-rich phase, and the interface locates around  $r = R + H_{\text{brush}}$  as expected. In order to quantify the degree of polymer interpenetration, we define the interfacial width as

$$w_I = -\frac{\phi_g(0)}{\phi'_g(r_{1/2})} \quad (\text{C1})$$

which is the brush density at the grafting surface,  $\phi_g(0)$ , divided by minus of the slope at  $r_{1/2}$  where the brush density is  $\phi_g(0)/2$  [3–5].

Interfacial widths corresponding to the cases of Figure S2a are shown in Figure S2b. For the thinnest brush case, at  $H_{\text{brush}}/aN^{1/2} = 1$ , the density profile of grafted polymers exhibits a slow decay over a relatively long radial distance from the particle surface. As the brush becomes thicker, the density slope becomes steeper and the interfacial width decreases. For the case of the very thick brush ( $H_{\text{brush}}/aN^{1/2} = 10$ ), the interpenetration region becomes considerably narrow.

In general, it is advantageous for the free chains to penetrate into the brush to increase their translational entropy, and such behaviors are observed for spherical wet brushes [6]. For the case of polymer melt system, however, significant stretching entropy cost is imposed when the free chain penetration depth is comparable to the brush thickness, and the balance between these two effects determines the interfacial width. When the brush is sparsely grafted, and its thickness is comparable to  $aN^{1/2}$ , free polymers can penetrate into the sparsely grafted brush in order to maximize the translational entropy of both types of polymers, and the resulting interfacial width becomes large. On the other hand, for a thick brush with a high grafting density, it is difficult for free polymers to penetrate into the highly stretched brush, and thus free polymers are expelled to reduce the conformational entropy cost, which results in a narrow interfacial width.

Figure S3 exhibits similar plots to those of Figure S2, but for different particle radii at fixed brush thickness  $H_{\text{brush}} = 2aN^{1/2}$ . It shows that unless the particle is extremely small, the effect of the particle size, or curvature, is not significant, as seen from density profiles and interfacial width. We expect that brushes on smaller particles behave as if the effective brush thickness is smaller than its actual value because, at fixed brush thickness, systems with higher curvature (or small particle size) provide extra space for grafted polymers to

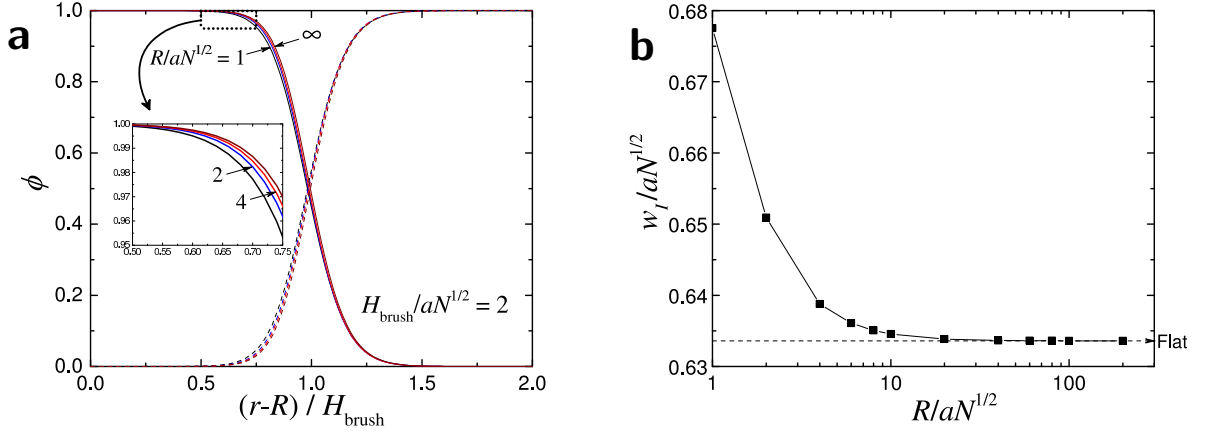


Figure S3: (a) Density profiles of grafted (solid lines) and free (dashed lines) polymers for the system of different particle radii  $R/aN^{1/2}=1, 2, 4$ , and  $\infty$  (flat brush) at fixed brush thickness  $H_{\text{brush}} = 2aN^{1/2}$  and  $\alpha = 1$ . The colored lines are difficult to distinguish because the convergence to the flat brush case is rapid. As seen in the inset, the lines are closely placed in the order of  $R/aN^{1/2}=1, 2, 4$ , and  $\infty$ . (b) Interfacial width  $w_I$  plotted as a function of  $R$ . The converging value corresponding to the flat brush case is denoted by a dashed arrow.

swell. It means smaller particles have more rooms to reduce the stretching entropy cost of the grafted chains when penetration of free chains occurs. As a consequence, the interfacial width must increase as the particle size decreases. Even though Figure S3b exhibits such a trend, the particle size must be extremely small ( $R < aN^{1/2}$ ) in order to observe a significant effect. At reasonable  $R$  values, the difference is very difficult to observe, and the convergence to the flat brush case ( $R = \infty$ ) is very rapid.

The morphology of the brush is determined not only by the system geometry but also by  $\alpha$ , the molecular weight ratio of polymers. We expect that for the mixture of grafted chains of length  $N$  and free chains of length  $\alpha N$ ,  $\alpha$  is the most dominant factor determining the interpenetration of the polymer chains [4, 7, 8]. In order to examine this effect, we choose radius  $R = 2aN^{1/2}$  and brush thickness  $H_{\text{brush}} = 2aN^{1/2}$  as our standard geometric parameters, and the density profiles at various  $\alpha$  values are plotted in Figure S4a. Also, the interfacial width is plotted as a function of  $\alpha$  in Figure S4b.

The extreme case,  $\alpha = 0.2$ , is close to a brush in solvents, and the density profile of grafted polymers exhibits a slow decay over a long radial distance from the particle surface. It implies that at small  $\alpha$ , the translational entropy of free polymers prevails conformational entropy of brush polymers, and thus free polymers penetrate deep into the brush and essentially form

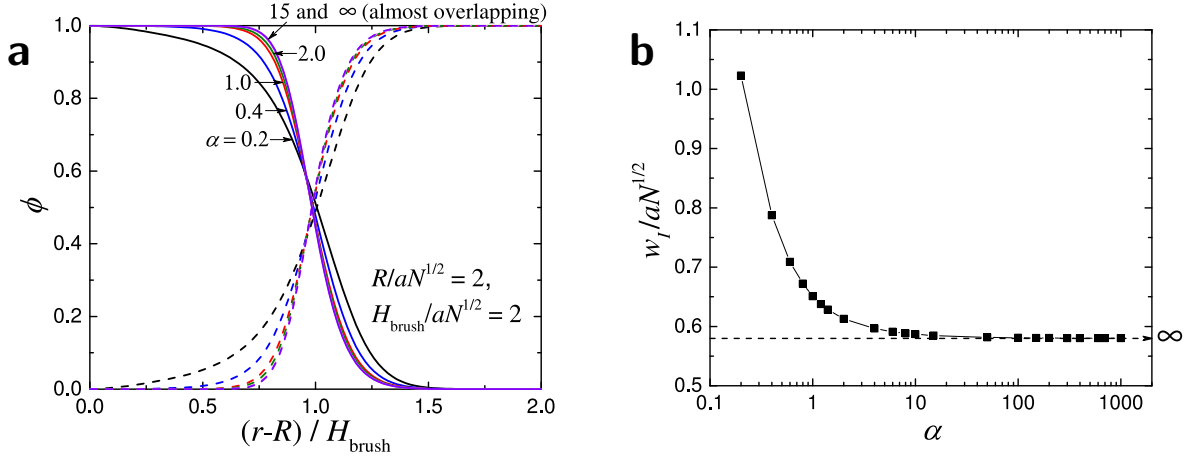


Figure S4: (a) Density profiles of grafted polymers ( $\phi_g$ , solid lines) and free polymers ( $\phi_f$ , dashed lines) for our standard system geometry with  $R = 2aN^{1/2}$  and  $H_{\text{brush}} = 2aN^{1/2}$  at  $\alpha$  values from 0.2 to infinity. (b) Interfacial width  $w_I$  plotted as a function of  $\alpha$  in a logarithmic scale. The converging value for the  $\alpha \rightarrow \infty$  case is denoted by a dashed arrow.

a brush in the wetting regime. As  $\alpha$  increases, the translational entropy of free polymers reduces and segregation of the brush and free chains becomes more prominent. At larger  $\alpha$ , the brush essentially goes into a dewetting brush regime, but the conformational entropy of the free chains remains finite and interpenetration of free chains never vanishes. Rather, the density profile approaches a hyperbolic tangent like shape in the limit  $\alpha$  goes to infinity. Convergence to the dewetting brush regime is so fast that above  $\alpha = 2$ , it almost converges to the limiting case of infinitely long homopolymers. Lines are very closely spaced, and the  $\alpha = 15$  line is practically within the line width of the limiting curve.

According to the interfacial width plot (Figure S4b), transition from wetting (e.g.,  $\alpha = 0.2$ ) to dewetting (e.g.,  $\alpha = 4$ ) brush is accompanied by the decrease of the interfacial width as expected. In experiments, molecular weight ratio  $\alpha$  is more easily controllable than the geometry, and it is notable that starting from our standard parameters of  $R = 2aN^{1/2}$ ,  $H_{\text{brush}} = 2aN^{1/2}$  and  $\alpha = 1$ , the change of parameter  $\alpha$  induces most dramatic interfacial width change. At high enough  $\alpha$ , above 4, penetration of polymers seems less dependent on the  $\alpha$  value, converging to the infinite  $\alpha$  case.

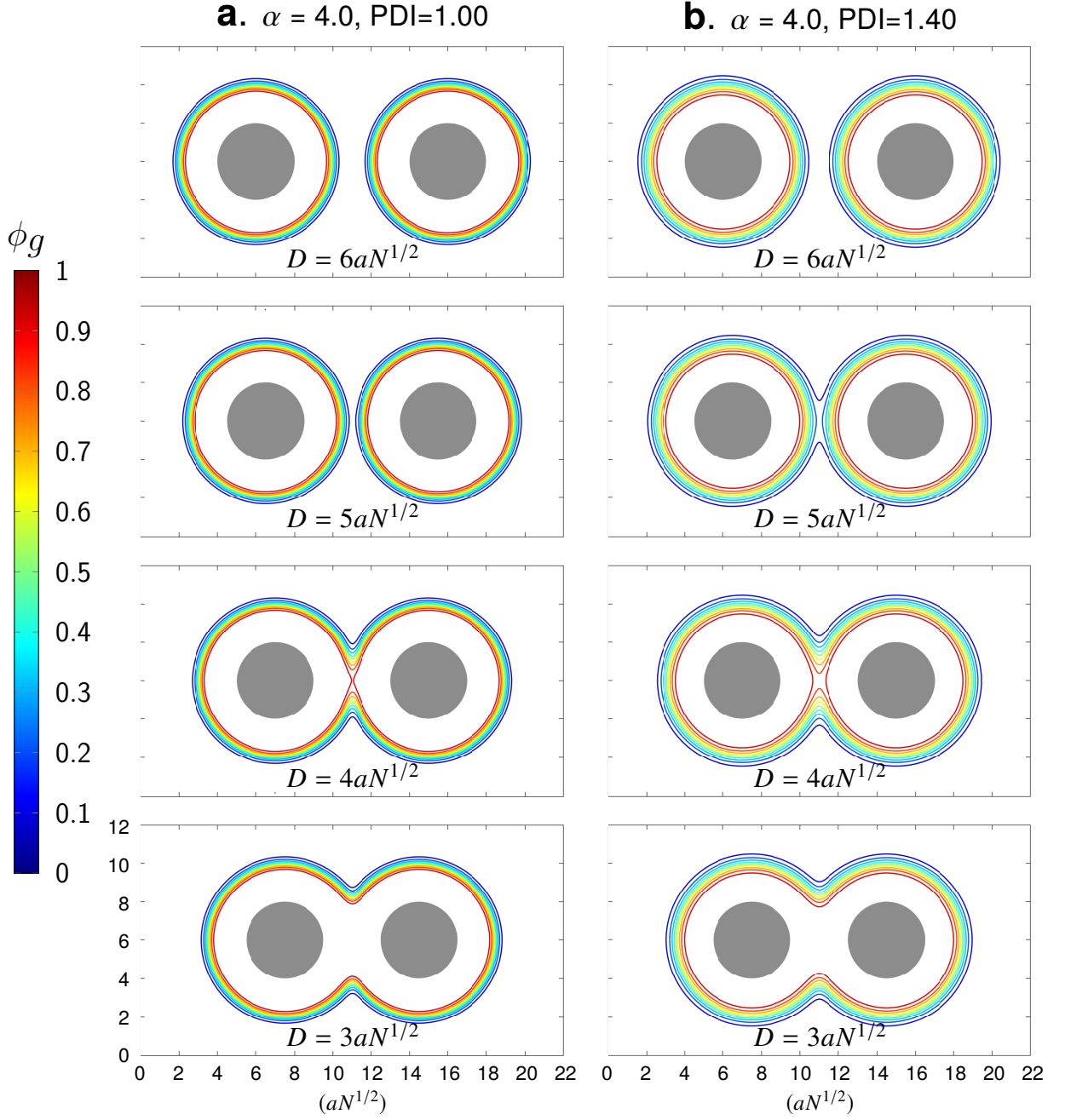
D. Contour Plots at  $\alpha = 4$ 

Figure S5: Contour plots of grafted polymer segment density,  $\phi_g$ , of (a)  $\alpha = 4.0$  and monodisperse (PDI = 1.00), and (c)  $\alpha = 4.0$  and polydisperse (PDI = 1.40) brushes calculated for two identical particles (gray circles) of radius  $R = 2aN^{1/2}$  and brush thickness  $H_{\text{brush}} = 2aN^{1/2}$ , separated by various interparticle distances  $D$ . Ten curvilinear contour lines are drawn at each plot to represent grafted polymer density from 0 (blue) to 0.9 (red).

### E. SCFT of End-fixed Brushes

The SCFT formulation in section B assumes that the grafted chain ends can float on the particle surface. Even when the chain ends are attached to the particle surface with strong chemical bonds, most procedures for deriving SCFT equations remain the same and only a few modifications to the SCFT equations are required [6, 9].

The segment density of chains grafted to particle one,  $\phi_{g1}(\mathbf{r})$ , is still obtained by calculating eq (20) in the main text, but there exists one exception that the initial condition of  $q_{g1}^\dagger$  is modified to

$$q_{g1}^\dagger(\mathbf{r}, 1) = \frac{V_{g1}\delta(r - R)}{4\pi R^2 q_{g1}(\mathbf{r}, 1)} \quad (\text{E1})$$

With this initial condition, brush chains are now uniformly grafted over the particle surface with surface density  $\sigma_0 \equiv n_g/8\pi R^2$ . After obtaining all the segment densities and mean potential fields, the free energy for the end-fixed brush case becomes

$$\frac{F}{k_B T} = n_f \ln \left( \frac{V_f}{Q_f[w]} \right) - 2\sigma_0 \int d\mathbf{r} \delta(r - R) \ln(q_g(\mathbf{r}, 1)) - \frac{\rho_0}{N} \int d\mathbf{r} w(\mathbf{r}) (\phi_g(\mathbf{r}) + \phi_f(\mathbf{r})) \quad (\text{E2})$$

### F. Contour Plots for Chain End Types

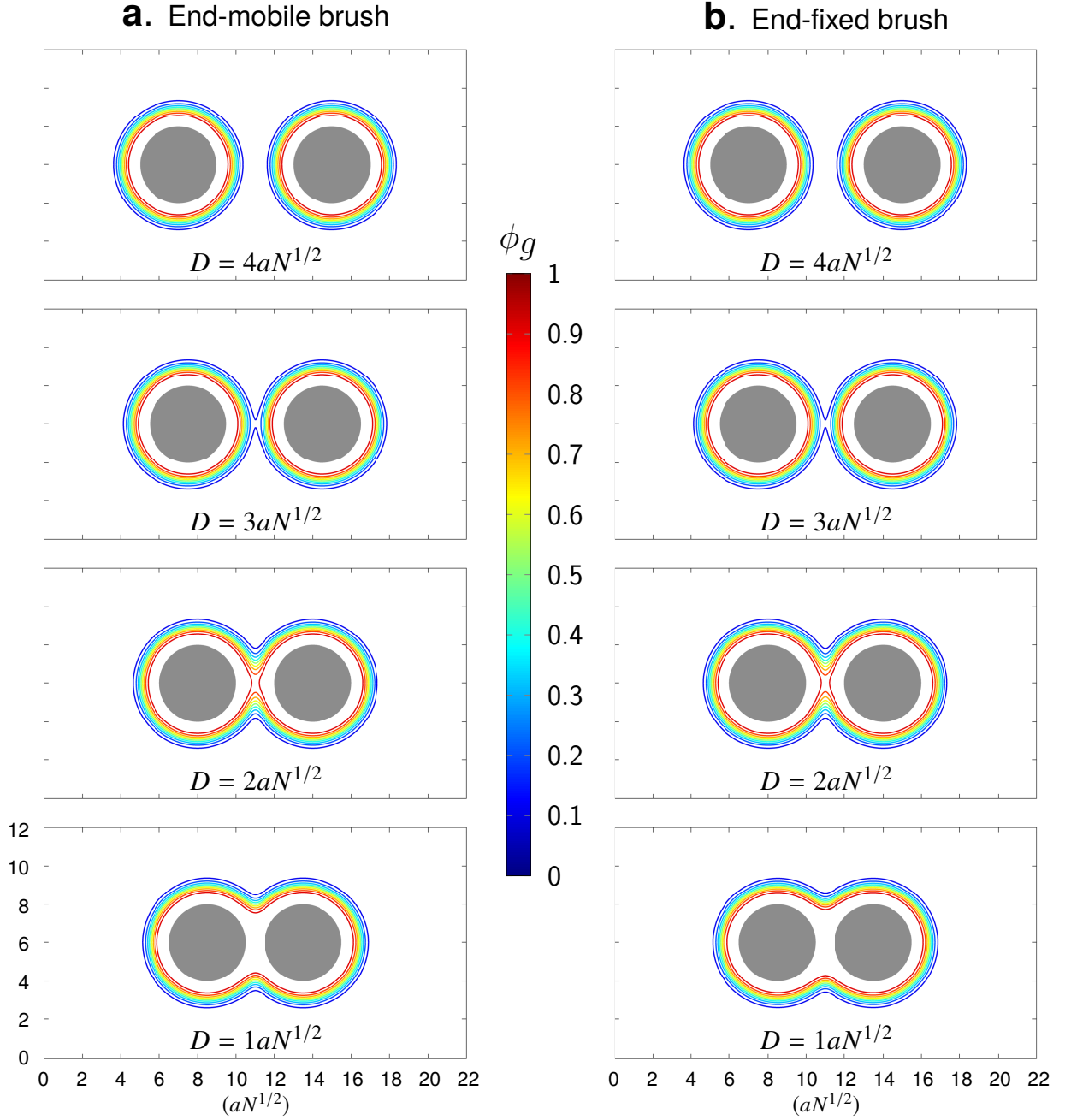


Figure S6: Contour plots of grafted polymer segment density,  $\phi_g$ , of (a) end-mobile and (b) end-fixed brushes at various interparticle distances  $D$  with the system geometry  $R = 2aN^{1/2}$ ,  $H_{\text{brush}} = aN^{1/2}$  and  $\alpha = 10$  which corresponds to the green line in Figure 7b of the main text.

- 
- [1] M. Yoo, S. Kim, J. Lim, E. J. Kramer, C. J. Hawker, B. J. Kim and J. Bang, Facile Synthesis of Thermally Stable Core–Shell Gold Nanoparticles via Photo-Cross-Linkable Polymeric Ligands. *Macromolecules*, 2010, **43**, 3570–3575.
- [2] S. Kim, M. Yoo, N. Kang, B. Moon, B. J. Kim, S.-H. Choi, J. U. Kim and J. Bang, Nanoporous Bicontinuous Structures via Addition of Thermally-Stable Amphiphilic Nanoparticles within Block Copolymer Templates. *ACS Applied Materials & Interfaces*, 2013, **5**, 5659–5666.
- [3] M. W. Matsen, in *Soft Matter*, ed. G. Gompper, M. Schick, Wiley-VCH, Weinheim, 2006, vol. 1.
- [4] D. M. Trombly and V. Ganesan, Curvature effects upon interactions of polymer-grafted nanoparticles in chemically identical polymer matrices. *J. Chem. Phys.*, 2010, **133**, 154904.
- [5] J. U. Kim, Y.-B. Yang and W. B. Lee, Self-Consistent Field Theory of Gaussian Ring Polymers. *Macromolecules*, 2012, **45**, 3263–3269.
- [6] J. U. Kim and M. W. Matsen, Interaction between Polymer-Grafted Particles. *Macromolecules*, 2008, **41**, 4435–4443.
- [7] M. W. Matsen and J. M. Gardiner, Autophobic dewetting of homopolymer on a brush and entropic attraction between opposing brushes in a homopolymer matrix. *J. Chem. Phys.*, 2001, **115**, 2794–2804.
- [8] I. Borukhov and L. Leibler, Enthalpic Stabilization of Brush-Coated Particles in a Polymer Melt. *Macromolecules*, 2002, **35**, 5171–5182.
- [9] J. U. Kim and M. W. Matsen, Positioning Janus Nanoparticles in Block Copolymer Scaffolds. *Phys. Rev. Lett.*, 2009, **102**, 078303.